Progress in Organic Coatings 76 (2013) 1556–1566

Contents lists available at SciVerse ScienceDirect

Progress in Organic Coatings

journal homepage: www.elsevier.com/locate/porgcoat

A modelling study of the visco-elastic behaviour of polyester-based coil coatings☆

I. Giannakopoulos*, A.C. Taylor

Department of Mechanical Engineering, Imperial College London, South Kensington Campus, London SW7 2AZ, UK

ARTICLE INFO

Article history:
Received 1 May 2013
Received in revised form 18 June 2013
Accepted 24 June 2013
Available online 20 July 2013

Keywords:
Coil-coatings
Viscoelasticity
Modelling tensile behaviour

ABSTRACT

The time and temperature dependence of the mechanical response of a series of polyester-based hexa(methoxymethyl)melamine cross-linked coil coatings was investigated. Small strain experiments such as dynamic mechanical analysis and stress relaxation are used to determine the parameters required for time–temperature superposition and for the determination of the relaxation spectra of the materials. Tensile tests at a range of temperatures and strain rates are used to show that time–temperature superposition can be successfully extended to cover the ultimate properties of the paints (i.e. those at fracture). Finally, a hybrid visco-elastic/hyper-elastic model is used to capture the tensile stress–strain response of the paints. The success of the visco-elastic component of the model is demonstrated at strains up to 5%, while at larger strains the model behaves best when the experimental behaviour of the material approaches that of rubber, with the fit becoming worse when the mechanical response is that of a ductile plastic.

1. Introduction

Coil-coating refers to the pre-painting of metal strips, which are subsequently stored as coils, to be formed at a later stage into the shape of the final product. The method is particularly popular with the construction, the automotive and electrical appliances industries, offering significant advantages both in terms of cost and of environmental impact [1,2]. As at the stage of forming the metal panels are already painted, the coating needs to be able to withstand the same level of deformation as the metal substrate without cracking or peeling away. A good understanding of the mechanical properties of the coating is therefore necessary for the production of optimal paint formulations, and for the prediction of the formability of the paint during the forming stage. Due to the requirement for high strength while maintaining a sufficiently low viscosity to facilitate application, coil coatings are generally based on heat-curing thermoset binders, most prominently polyesters cross-linked with hexa(methoxymethyl)melamine [2]. Moreover because coil coatings are required to withstand substantial strains at the forming stage, their T_g is generally tuned to be close to the expected forming temperature. As a result, coil coatings tend to be highly visco-elastic around room temperature, so their mechanical properties depend strongly on both temperature and testing rate. A good understanding of the visco-elastic nature of these paints is therefore imperative.

In the industry-specific literature the visco-elasticity of coil-coatings is acknowledged and indeed considered as a factor affecting the formability of different paint formulations [3–5]. However, to the authors' knowledge, there exist no systematic studies of the visco-elasticity of such systems or attempts to model their mechanical behaviour using the constitutive equations available for polymers. On the other hand, visco-elastic and hyper-elastic material models have been used to capture the behaviour of artists' paints with promising results [6–8]. In the present study it is sought to investigate the temperature, rate and strain dependent behaviour of a series of polyester-based HMMM-cross-linked coil coatings. For this, a simple hyper-elastic/visco-elastic model is used with the focus being primarily on the experimental determination of the model constants, and on the interpretation of these constants in terms of the chemical structures of the paints. These results should prove particularly useful for future studies, as they provide a material model which can be used with finite element modelling to predict the forming process of coated metal panels. A short introduction into the relevant theory is given, followed by a description of the experimental procedure and of the paint formulations. The results are presented with a particular emphasis on their justification by considering the chemical structure of the materials.

* Corresponding author. Present address: Department of Engineering Science, University of Oxford, 9 Parks Road, OX1 3PJ, UK. Tel.: +44 18 65 2738 11.
E-mail address: ioannis.giannakopoulos@eng.ox.ac.uk (I. Giannakopoulos).

0300-9440/$ – see front matter © 2013 The Authors. Published by Elsevier B.V. All rights reserved.
http://dx.doi.org/10.1016/j.porgcoat.2013.06.010

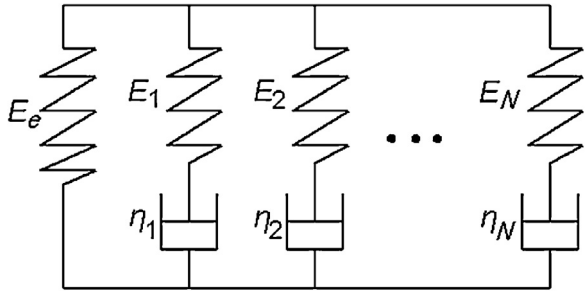

Fig. 1. Schematic diagram of generalised Maxwell model with a spring and N Maxwell elements in parallel. Each Maxwell element, i, corresponds to a relaxation time of $\tau_i = \eta_i/E_i$.

2. Modelling studies

2.1. Rate dependence at small strains

At small strains the time and temperature dependent mechanical behaviour of polymers is very adequately captured by the standard theory of linear visco-elasticity as given by Ferry [9]. A common approach in modelling visco-elastic effects involves the use of spring and dashpot mechanical analogues. Here, a standard mechanistic model of visco-elasticity is used, where a spring (linear elastic, time-independent element) is connected in parallel with a number of Maxwell elements (visco-elastic, time dependent) as shown in Fig. 1. Each Maxwell element is associated with a unique relaxation time, τ, defined as:

$$\tau = \frac{\eta}{E} \tag{1}$$

where E is the Young's modulus of the spring and η is the viscosity of the dashpot in the Maxwell element.

For the case of a linear visco-elastic solid subjected to a known strain history, $\varepsilon(s)$ within a time interval, $0 < s < t$, the stress can be predicted as a function of time, t, as [10]:

$$\sigma(t) = E(0)\varepsilon(s)g_e + E(0)\sum_{1}^{N}\int_{0}^{t} g_i \exp\left(-\frac{t-s}{\tau_i}\right)\frac{d\varepsilon}{ds}ds \tag{2}$$

where N is the number of Maxwell elements, $E(0)$ is the instantaneous (glassy) modulus of the material, $g_i = E_i/E(0)$ are the weights of each Maxwell element i and $g_e = E_e/E(0)$ the weight of the equilibrium spring where E_e is the relaxed equilibrium (rubbery) modulus of the material. The number of Maxwell elements used is arbitrary and is chosen as required in order to accurately capture the material behaviour. A distribution of 18 relaxation times (Maxwell elements) was used, and this was found to provide good agreement with the experimental data.

The distribution of relaxation times, g_i, will depend on the microstructure of the polymer, for example on the molecular weight of the relaxing segments and on the cross-link density of the network. As each polymer contains a finite number of relaxing segments, a discrete distribution of relaxation times is justified [11]. However, it is convenient to propose analytical solutions for the distribution of relaxation times, where it is assumed to be continuous. Here it was found useful to constrain the g_i to take values from such a continuous distribution of relaxation times. This approach on one hand made it easier for the model to converge to a numerical solution, and on the other it facilitated the comparison between distributions obtained from different samples, as the shape of the distribution remained essentially the same with only the breadth and the position of the peak changing.

Several analytical equations have been used to capture relaxation, including the log-normal (see [12] for example) and Cole–Cole [13,14] distributions. For this study, a generalised form of the Cole–Cole distribution [15] was used to fit the data, with the distribution of relaxation times, $h(z)$, given as:

$$h(z) = \frac{1}{\pi}\frac{z^{c-d}\left\{\sin[(d-c)\pi] + z^c \sin d\pi\right\}}{1 + 2z^c\cos(c\pi) + z^{2c}} \tag{3}$$

where c and d are constants which determine the shape of the relaxation with $c \le d \le 1$, and $z = \tau/\tau^*$ where τ^* is a characteristic relaxation time.

2.2. Time–temperature superposition

Eq. (2) can predict the stress in a polymer that is subjected to a known strain history as a function of time. However it is well known that temperature will also affect the mechanical response of polymers and what is more the effects of temperature and time are equivalent. Assuming that the material is thermorheologically simple (see [16] for a discussion), this equivalence is accurately captured at temperatures above T_g by the Williams–Landel–Ferry equation (Eq. (4)), that is derived from a consideration of the free volume present in polymers allowing chain segments to change their conformation and relax [17]:

$$\log\ \alpha_T = -\frac{C_1(T - T_{ref})}{C_2 + T - T_{ref}} \tag{4}$$

where C_1 and C_2 are constants, T_{ref} is a reference temperature (customarily taken at T_g), T is the temperature at which the data were collected, and

$$\alpha_T = \frac{t}{t_{ref}} \tag{5}$$

where t_{ref} is the time corresponding to the reference temperature, T_{ref}, and t is the time corresponding to temperature, T.

At temperatures below T_g stress relaxation takes place via smaller movements, such as movements of side-groups or very localised conformation changes along the polymer chains. Therefore a free volume approach can no longer capture the time–temperature equivalence of macroscopic behaviour, but rather an activation energy approach is followed in Eq. (6) by application of an Arrhenius type equation [18]:

$$\log\ \alpha_T = \frac{\delta H}{R}\left(\frac{1}{T} - \frac{1}{T_{ref}}\right)\frac{1}{2.303} \tag{6}$$

where δH is the activation energy required for the relaxation, and R is the ideal gas constant (taken as 8.314 J/mol K).

It follows that if the distribution of relaxation times at a reference temperature is known, the mechanical response of a polymer can be predicted at any temperature by simply shifting the g_i along the time axis according to Eqs. (4) and (6). This means that with changing temperature the shape of the distribution of relaxation times stays the same, with only its position along the time axis changing.

2.3. Prediction of response at large strains

The linear visco-elastic analysis shown above assumes that the sample is subjected to strains which are small enough for entropic effects from changes in chain conformation to be neglected. At larger strains, however, the contribution from large-scale conformational changes (chain uncoiling and stretching) to the stress–strain behaviour cannot be neglected, and this needs to be accounted for in Eq. (2). At this point an assumption is usually made that the stress response can be decomposed into two separate components: one that is solely time-dependent (visco-elastic part)

and one that is strain-dependent (hyper-elastic part) [19]. This can be incorporated into Eq. (2) by rewriting it as [10]:

$$\sigma(t) = \sigma_0 g_e + \sum_1^N \int_0^t g_i \exp\left(-\frac{t-s}{\tau_i}\right) \frac{d\sigma_0}{ds} ds \quad (7)$$

where σ_0 is the hyper-elastic time-independent component of the stress. The integral in Eq. (7) was calculated here using the approximate solution given by Goh et al. [10].

Various theories have been proposed which capture the hyper-elastic behaviour of rubbers, and reviews of the main theories can be found in [20–22]. For the purposes of this study the Ogden model [23] was found to provide good results with a relatively small number of optimisation parameters. Ogden proposed a strain energy function which depends on the principal stretches of the material (λ_1, λ_2 and λ_3) as:

$$W_{\text{Ogden}} = \sum_j \frac{\mu_j}{a_j}(\lambda_1^{a_j} + \lambda_2^{a_j} + \lambda_3^{a_j} - 3) \quad (8)$$

where μ_j and α_j are constants with

$$\sum \mu_j a_j = 2G \quad (9)$$

where G is the shear modulus of the material calculated as $G = E(0)/3$ where a Poisson's ratio of 0.5 is implied. Another requirement is that $\mu_j a_j > 0$ for all j, which ensures that the model predictions remain physically realistic [24,25]. This point is discussed in Section 5.

For the case of uniaxial extension the true stress acting on the material is given by:

$$\sigma_0 = \lambda \sum_j \mu_j(\lambda^{a_j - 1} - \lambda^{-(0.5a_j+1)}) \quad (10)$$

where the stretch ratio, λ, can be expressed in terms of the strain, ε, as $\lambda = 1 + \varepsilon$.

3. Materials and manufacturing

Two different polyester binders were used in this study, referred to as PE1 and PE2. Binder PE1 was a branched polyester similar to these used for coil coating applications, with a molecular weight, M_n, of 4200 g/mol. Binder PE2 was a non-branched, higher molecular weight (M_n = 8400 g/mol) modification of PE1. The two binders were heat-cured with hexa(methoxymethyl)melamine (HMMM). As a result of the elimination of branching, PE2 also had a lower functionality than PE1 (on average 2 OH sites per chain, compared to an average of 3.6 OH sites in the case of PE1), and therefore binder PE1 is expected to give a paint of higher cross-link density than PE2, when the same HMMM concentration is used. In the case of binder PE1, three different binder:cross-linker ratios were used, 90:10, 80:20 and 70:30 by weight. The resulting paints will be referred to as PE1H10, PE1H20 and PE1H30. Binder PE2 was cross-linked with HMMM at an 80:20 ratio (PE2H20). The paints were applied on PTFE-coated steel panels using a draw-down bar. They were cured to a peak metal temperature (PMT) of 232 °C inside a gas oven. The oven temperature was 265 °C, and a dwell time of 30 s was required to reach the desired PMT. The panels were subsequently cooled by resting on a magnetic plate for a period of a few seconds. The resulting paint films had an approximate thickness of 20–30 μm when peeled off the PTFE-coated panels, and samples were cut using a razor blade.

4. Experimental procedures

4.1. Thermomechanical characterisation

Samples were tested using differential scanning calorimetry (DSC) in order to determine their glass transition temperatures. For this, a TA Q2000 DSC (TA Instruments, USA) was used. Paint samples of 5–10 mg were put into hermetically closed aluminium pans and were subjected to a heat–cool–heat cycle between −30 and 100 °C at a heating rate of 10 °C/min.

Dynamic mechanical analysis (DMA) was performed using a Tritec 2000 DMA in tensile mode, at temperatures between −20 and 120 °C and a heating rate of 2 °C/min. During the heating ramp, the samples were subjected to a frequency scan where three different frequencies of 0.1, 1 and 10 Hz were used. It is recognised that it is not ideal to simultaneously change the temperature and the testing frequency. However, the DMA was not equipped with an automatic cooling system and therefore it was not possible to reliably maintain isothermal conditions, especially at low temperatures. This point is further discussed in Section 5, where it is shown that the choice of isothermal or temperature ramp conditions did not affect the results greatly. The test amplitude was set to approximately 0.1–0.2% strain, while an initial pre-load of 0.3 N was applied to the samples. The 'auto-tension' option was selected in the Tritec 2000 software, which varies the ratio of static to dynamic force applied on the samples, and was found to provide the best results for the thin films investigated in this study. The samples were rectangular, approximately 5 mm in width with a free length between the clamps of 5 mm.

4.2. Tensile testing

Tensile tests were performed on rectangular strips of the paint, of approximately 60 mm × 6 mm, using an Instron 4301 (Instron, USA) universal testing machine with a 100 N load-cell. Temperature and humidity control was achieved with an environmental chamber previously developed at Imperial College London [26]. To achieve a better grip on the samples within the tensile clamps, paper end-tabs were bonded to the samples using a commercial cyanoacrylate adhesive leaving a free length of 40 mm. Samples were loaded in tension until failure at a displacement rate of 5 mm/min and at a wide range of temperatures around the T_g of the paints. Paint PE1H20 was subjected to additional tests at displacement rates 0.05, 0.5 and 50 mm/min. For all tests performed at temperatures above 10 °C the relative humidity was kept constant at 50%, while it proved impossible to consistently maintain a 50% relative humidity at lower temperatures.

The same experimental set-up was used to perform relaxation tests. Samples were loaded to a strain of approximately 1% at which point the cross-head movement was stopped and the stress relaxation was monitored as a function of time. The displacement rate to the constant 1% strain was set to 50 mm/min. The temperature used for the relaxation tests was equal to the T_g (DSC) of the samples, and the relative humidity was again maintained constant at 50%.

5. Results and discussion

5.1. Determination of glass transition temperature

The variation in HMMM content did not affect the position of the glass transition measured using DSC, as all three PE1-based paints had a common T_g of approximately 35 °C, see Table 1. The T_g of paint PE2H20 was significantly lower at 17 °C. A more detailed presentation of these data, as well as a discussion on their correlation to paint formulation and chemical structure, will be given in a future

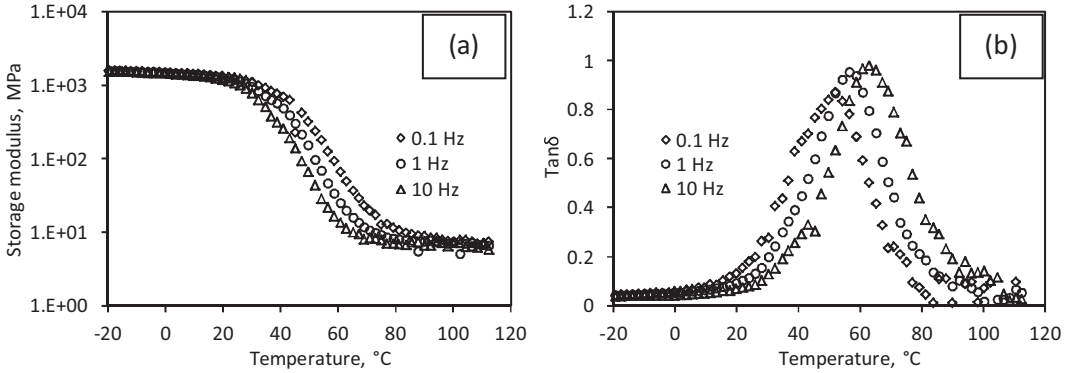

Fig. 2. Storage modulus (a) and tan δ (b) versus temperature, obtained from multi-frequency DMA test of formulation PE1H20.

Table 1
Glass transition temperature and cross-link density of paint systems.

Formulation	T_g (DSC) (°C) (±2)	Cross-link density (10^{-3} mol/cm^3)
PE1H10	35	0.64 ± 0.02
PE1H20	36	0.93 ± 0.06
PE1H30	35	2.08 ± 0.16
PE2H20	17	0.47 ± 0.09

article dealing specifically with the experimental characterisation of the materials.

5.2. Time–temperature superposition (small strains)

Characteristic multi-frequency DMA data of PE1H20 are shown in Fig. 2. As expected, an increase in frequency results in a shift of the tan δ peak to higher temperatures, from 52 °C at 0.1 Hz, to 57 °C at 1 Hz and 63 °C at 10 Hz, whereas the behaviour in the glassy and rubbery regions is seen to be time-independent. The modulus at the rubbery plateau, E_e, can be used to calculate the cross-link density, ν_e, of the paints as:

$$\nu_e = \frac{E_e}{3RT_e} \tag{11}$$

where R is the gas constant and T_e is the temperature at the rubbery plateau. The cross-link densities of the paints, calculated from Eq. (11), are shown in Table 1. For the calculation, E_e was taken as the average value of storage modulus between 80 °C and 120 °C from DMA, while T_e was taken as the average temperature within the same range, i.e. 100 °C. A continuous increase in cross-link density is seen with the addition of cross-linker (HMMM) for the paints using the PE1 binder. The relatively low value measured for PE2H20

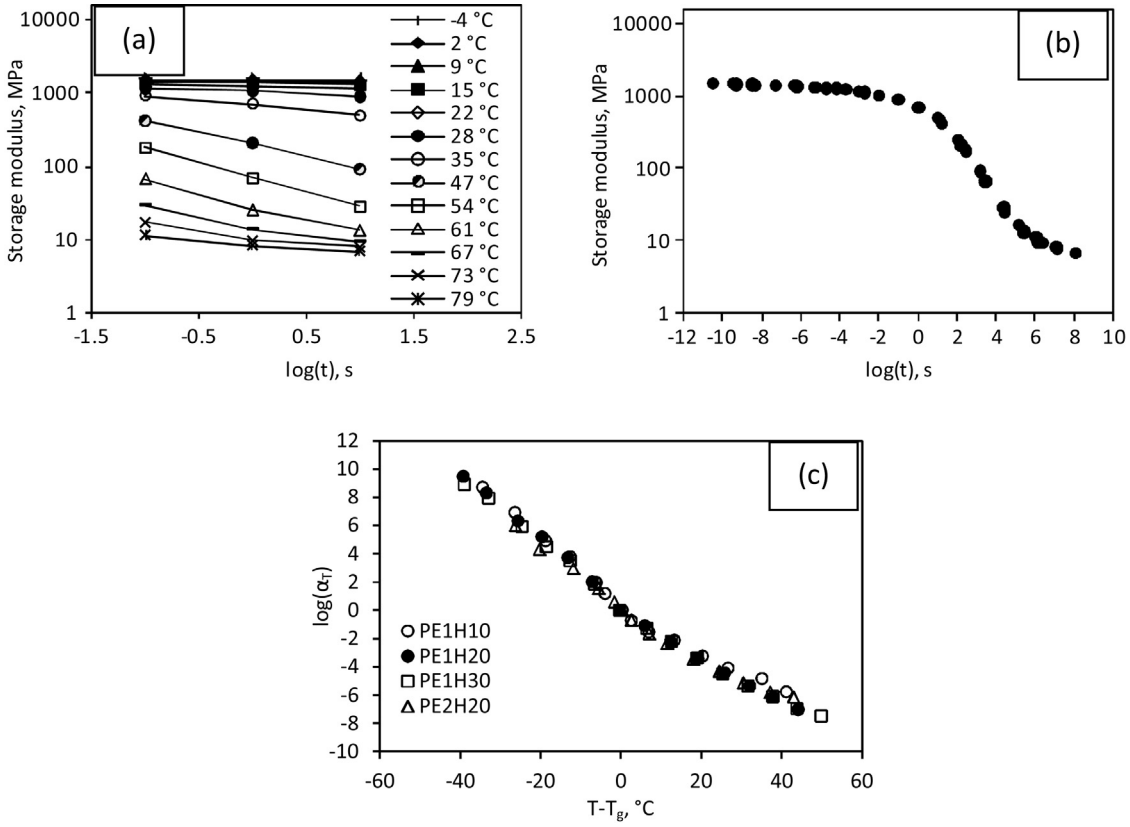

Fig. 3. Isotherms (a) and master-plot (b) of storage modulus versus the logarithm of time for PE1H10-30 and PE2H20. In (c) the logarithm of the paints' experimental shift factors is plotted versus $T - T_g$.

Table 2
Time–temperature superposition constants (δH, C_1 and C_2) applicable to all paint systems and paint-specific visco-elastic parameters ($E(0)$, E_e, τ^*, c and d).

TTS constants based on all available data			Paint-specific visco-elastic parameters					
δH (kJ/mol)	C_1	C_2 (K)	Formulation	$E(0)$ (MPa)	E_e (MPa)	τ^* (s)	c	d
395	17	76	PE1H10	2440	6	0.07	0.63	0.67
			PE1H20	2070	9	1.03	0.46	0.50
			PE1H30	2180	20	0.70	0.20	0.24
			PE2H20	1900	5	1.55	0.69	0.73

can be attributed to the non-branched nature and the lower functionality of this polyester.

Re-plotting the storage modulus data as isotherms versus the logarithm of time (taken as the inverse of frequency), see Fig. 3(a), and further rearranging with respect to the isotherm at 35 °C (selected for being approximately the glass transition temperature from DSC) provides a master plot of storage modulus spanning several decades of time at the reference temperature of 35 °C, see Fig. 3. A similar procedure was followed for the rest of the paint films, shifting the data with respect to the T_g measured using DSC. The shift factors required to achieve the superposition of the isotherms can then be plotted versus temperature as shown in Fig. 3(c). The time–temperature superposition (TTS) constants, C_1, C_2, and δH can then be obtained by fitting Eqs. (4) and (6) to the shift factors versus temperature plots. As seen from Fig. 3(c), at temperatures at an equal distance from T_g, the shift factors were very similar for all paints. It was therefore decided to calculate 'universal' values for the TTS constants based on the shift factors obtained from all the systems investigated in this study. These are shown in Table 2.

Additional tests were performed where samples of PE1H20 were subjected to frequency scans (0.1–10 Hz) under isothermal conditions at temperatures between 15 and 120 °C with the temperature increasing in 5 °C steps. The experimental set-up was found to maintain isothermal conditions with sufficient accuracy above 25 °C, while at lower temperatures small temperature increments in the order of 1 °C were observed during the frequency scan. The storage modulus master-plots and shift factors obtained under temperature-ramp and isothermal conditions are compared in Fig. 4. Clearly, the data obtained under the two different conditions agree well, so the application of a temperature ramp along with the frequency scan did not affect the values of the TTS constants presented here.

5.3. Time–temperature superposition (application to failure strain)

In the previous section, time–temperature superposition was applied to storage modulus data obtained within the linear visco-elastic limit of the tensile behaviour of the samples, i.e. at strains considerably smaller than 1%. It would be of interest to use the TTS constants obtained at these small strains to predict quantitatively the interdependence between time and temperature at large strains. For this, tensile tests were performed on samples of PE1H20 at four different temperatures (15, 25, 35 and 45 °C) and displacement rates (0.05, 0.5, 5 and 50 mm/min). The Young's modulus was determined as the slope of a linear regression fit to the stress–strain curve of each sample, between 0.2% and 0.8% strain. This definition was preferred instead of a secant modulus approach as it provides an averaged value minimising any effects of data-logging noise. The TTS constants given in Table 2 were used to shift the tensile Young's modulus values with respect to the 35 °C isotherm. The isotherms and the master curve obtained from the shift are shown in Fig. 5, where the time values correspond to the time at the point of measurement of the modulus. The superposition of the isotherms is seen to be good, even though it is acknowledged that the overlap of the points is clearly less than perfect in the time range between 0.1 and 1 s.

As the use of the TTS constants on small strain tensile data was encouraging, it was decided to extend the application of time–temperature superposition to ultimate properties. Master-plots of the failure stress and of the failure strain versus the logarithm of time to failure are shown in Fig. 6. Once more the shifting of the data-points was performed with respect to the 35 °C isotherm by the use of the TTS constants given in Table 2. A good overlap of the data is seen with some discrepancies observed at times between 10^2 and 10^4 s. These results show that the rate dependence of the failure stress and strain follow the rate dependence of the modulus at small strains, i.e. high loading rates result in a brittle response (low failure strain) while low loading rates result in a ductile and eventually rubbery response (high failure strains). Further, the successful application of time–temperature superposition for large strain properties means that, by performing tests over a modest range of temperatures, the ultimate properties of the paints can be obtained over a very broad range of strain rates. It is noted here however that this treatment assumes that the samples are not subjected to adiabatic heating during loading, i.e. that conditions remain isothermal during testing. This condition is generally not satisfied at high loading rates where the rate of heat transfer

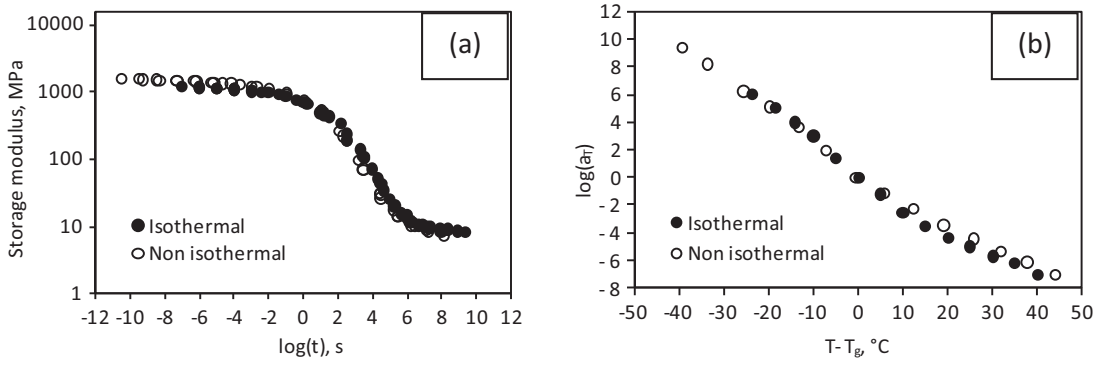

Fig. 4. Storage modulus master-plots (a) and shift factors (b) obtained from isothermal and temperature-ramp (non-isothermal) DMA of paint PE1H20.

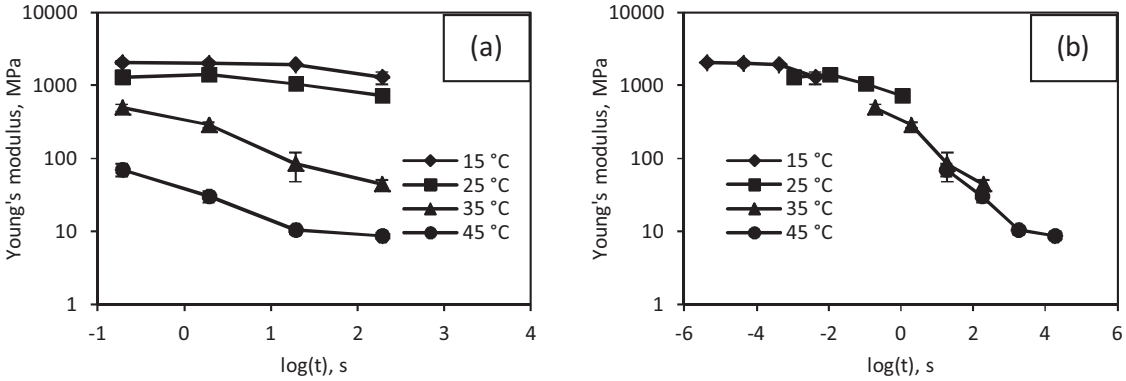

Fig. 5. Isotherms of Young's modulus versus the logarithm of time at the point of measurement (a), and master-plot of Young's modulus created by using the TTS constants determined from multi-frequency DMA data (b) for PE1H20.

from the sample to the environment is comparable to the time scale of the experiment (see [27] for example).

Notwithstanding possible discrepancies due to the effect of adiabatic heating, the equivalence of rate and temperature effects on the ultimate properties of polymers can be further shown with the use of failure envelopes, created initially by Smith [28]. Such a failure envelope is shown for paint PE1H20 in Fig. 7(a), where the logarithm of the failure stress normalised by the ratio of the test temperature over T_g is plotted versus the logarithm of the failure strain. The open circles correspond to data collected at multiple temperatures (0, 10, 20, 30, 40, 55 and 65 °C) and constant displacement rate (5 mm/min), while the filled circles correspond to tests performed at four different temperatures (15, 25, 35 and 45 °C) and displacement rates (0.05, 0.5 5, 50 mm/min). The data are seen to form a single envelope of failure points. Following the envelope clockwise corresponds to increasing the temperature or decreasing the displacement rate of the experiment.

A point of interest is the maximum observed in the failure strain of the paint seen in both Figs. 6(a) and 7(a). This maximum has been reported extensively [28–31] for polymers and has been proposed to occur where energy dissipation (through for example stress relaxation and chain uncoiling) reaches a maximum [32,33]. In temperature terms, this is expected to occur at or near the polymer's T_g. In Fig. 7(b) the failure envelopes of all paints are compared, where the failure stress is now further normalised by the cross-link density of each paint. For the PE1-based paints the maximum failure strain is seen to decrease with increasing HMMM content, while towards the low temperature/high rate regime (top left corner of graph), the failure stress normalised for cross-link density and testing temperature increases with decreasing concentration of HMMM. The failure envelope of the PE2-based paint generally lies outside the low HMMM content PE1-based paint, with a markedly larger maximum failure strain. These results demonstrate the significant decrease in the peak failure strain with increasing cross-link density, and agree well with the general trends of failure envelopes reported by Landel and Fedors [30].

5.4. Stress relaxation – determination of distribution of relaxation times

The time-dependent behaviour of the paints was further explored with the use of relaxation tests. Plots of the stress versus the logarithm of time are shown in Fig. 8. For the paints based on polyester PE1, an increase in the HMMM concentration results in broadening of the time required for the stress to relax. When the paint based on PE2 (with 20 wt% of HMMM) is compared to paint PE1H20, it is seen that the relaxation is quicker in the case of the PE2-based paint. It is proposed that the different breadths of the relaxation spectra are directly related to the cross-link densities of the paints, with increasing cross-link density resulting in a more gradual relaxation. This mirrors the effect of cross-link density on the broadness of the tan δ peak from DMA (results not shown here) and has been attributed to an increase in the diversity of the level of constraint seen by chain segments with increasing cross-link density [34,35].

Eq. (7), where $i = 18$, was used to fit the experimental relaxation data. After initial attempts to model the relaxation behaviour by incorporating a hyper-elastic function for the strain dependent part of Eq. (7), it was found that the fit was rather insensitive to the application of the hyper-elastic function. Thus, it was decided to ignore non-linear elasticity effects at the small strains over which the relaxation data were collected, and instead the strain dependent part of Eq. (7) was assumed to follow Hooke's law, i.e. $\sigma_0 = E\varepsilon$. In every case the glassy and rubbery moduli $E(0)$ and E_e were obtained directly from the DMA data (Fig. 2), while the characteristic relaxation time τ^*, and the constants c and d from the generalised

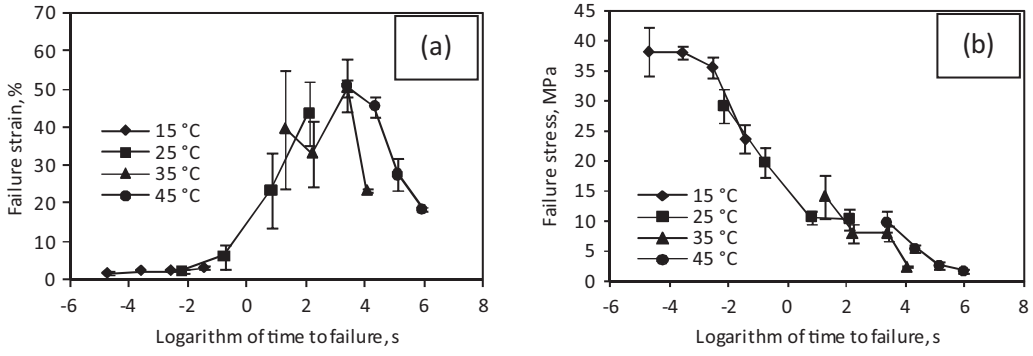

Fig. 6. Master-plots of failure strain (a) and failure stress (b) created by using the TTS constants determined from multi-frequency DMA data, for PE1H20.

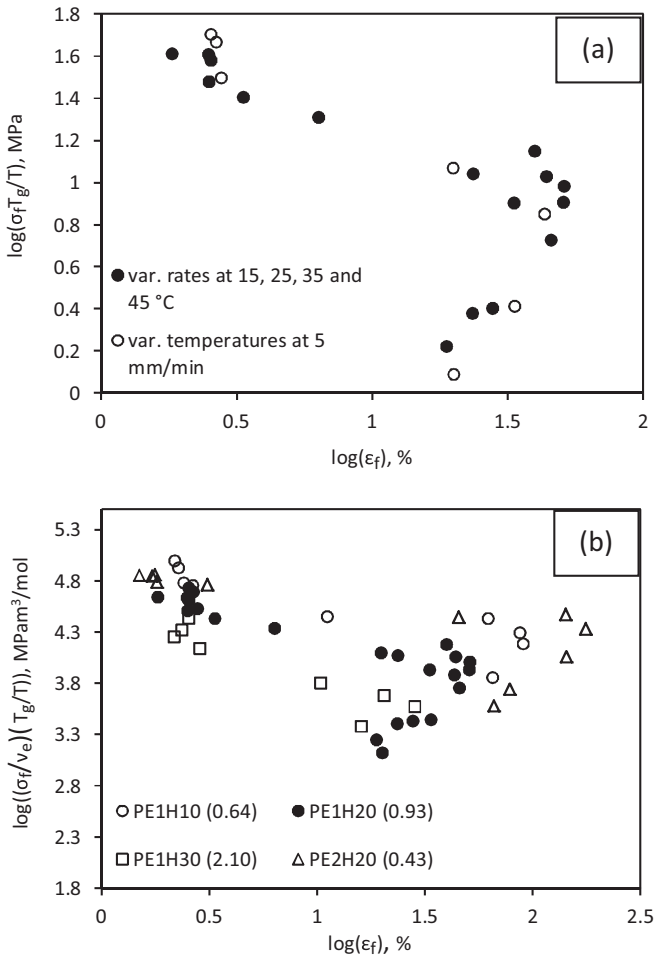

Fig. 7. Failure envelope of paint PE1H20 where the data were obtained at various temperatures and displacement rates (a) and comparison of the failure envelopes of all paint systems studied (b). The cross-link density in 10^{-3} mol/cm^3 is shown in brackets.

Cole-Cole equation were treated as optimisation parameters to obtain a good fit between model (Eq. (7)) and experimentally obtained relaxation data. The fit to the experimental data is seen in Fig. 8(a) while the corresponding distributions of relaxation times of the paints are shown in Fig. 8(b). The optimisation constants τ^*, c and d are given in Table 2. Parameters c and d control the shape of the spectra and their values reflect the increase in the width of the distribution of relaxation times with increasing cross-link density. The characteristic time, τ^*, represents the intercept of the short-time and long-time asymptotes of the distribution or the time where a local maximum can be observed in the spectra. The values of τ^* appear to be uncorrelated with cross-link density and when the time-range of the spectra is considered they are also seen to be quite similar for all paints. Roland [35] examined dielectric spectroscopy data and found the intermolecular relaxation time (which appears to be analogous to τ^* used here) to increase with cross-link density. However, in his study T_g was also found to increase with cross-link density whereas, here, T_g remains unaffected by the degree of cross-linking. For the purposes of this article, τ^*, is considered a curve-fitting parameter, as a detailed investigation of the relaxation mechanisms present in polymer networks was outside the scope of the present study. The good agreement between the measured and the calculated relaxation values was expected as the experimental data were used directly for the calibration of constants τ^*, c and d.

5.5. Modelling of uniaxial tension data

Following the determination of the TTS constants and of the distributions of relaxation times, it was attempted to model the full tensile behaviour of the paints at various temperatures. This was done by use of Eq. (7), as in the case of the relaxation data, however now the Ogden model (Eq. (10)) was used to determine σ_0, in recognition that at large strains (above a few percent) hyper-elastic effects cannot be ignored. A check was performed first regarding the validity of the underlying assumption in Eq. (7) that the effects of strain and time on the mechanical behaviour are separable. Smith [19] has proposed that for this assumption to hold, iso-strain values of the logarithm of stress obtained at different strain rates should give a series of parallel curves when plotted versus the logarithm of time. Such plots were constructed from the multiple displacement rate data of paint PE1H20, at temperatures of 15, 25, 35 and 45 °C, and are shown in Fig. 9. The isostrains are generally parallel, which suggests that the mechanical response of the paints can be separated into a purely time-dependent and a purely strain-dependent component. The shortening of the distance separating the iso-strain curves, for example for strains between 1.7% and 2.5% in the case of the 15 °C plot (Fig. 9(a)), or at short times and strains between 5% and 20% in the case of the 35 °C plot (Fig. 9(c)), can be attributed to the presence of a yield point and of an extended cold-drawing behaviour respectively.

Returning to the modelling of the tensile behaviour of the paints, in order to fit Eq. (7) to the experimental data, two sets of parameters are required: one that is related to the visco-elastic part of the behaviour and one related to the hyper-elastic part. The visco-elastic parameters have already been obtained through stress

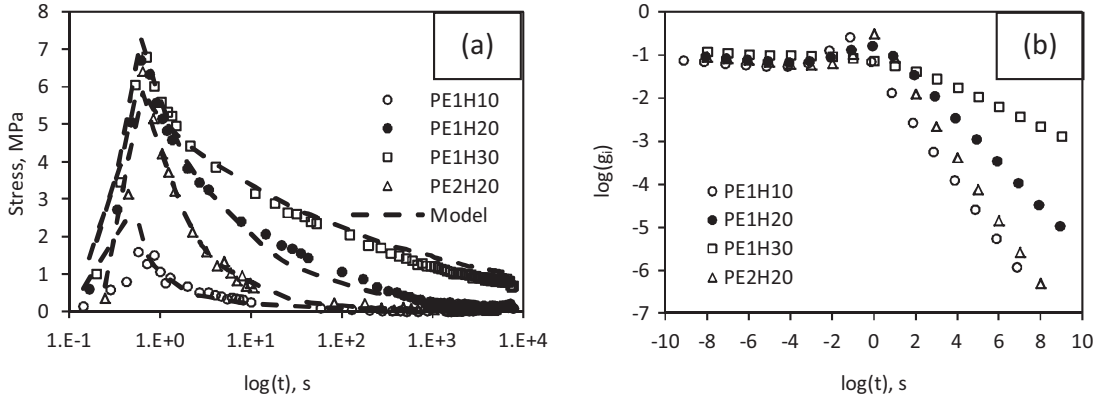

Fig. 8. In (a) relaxation data are shown, obtained experimentally and from Eq. (7). Also shown are the resulting distributions of relaxation times (b).

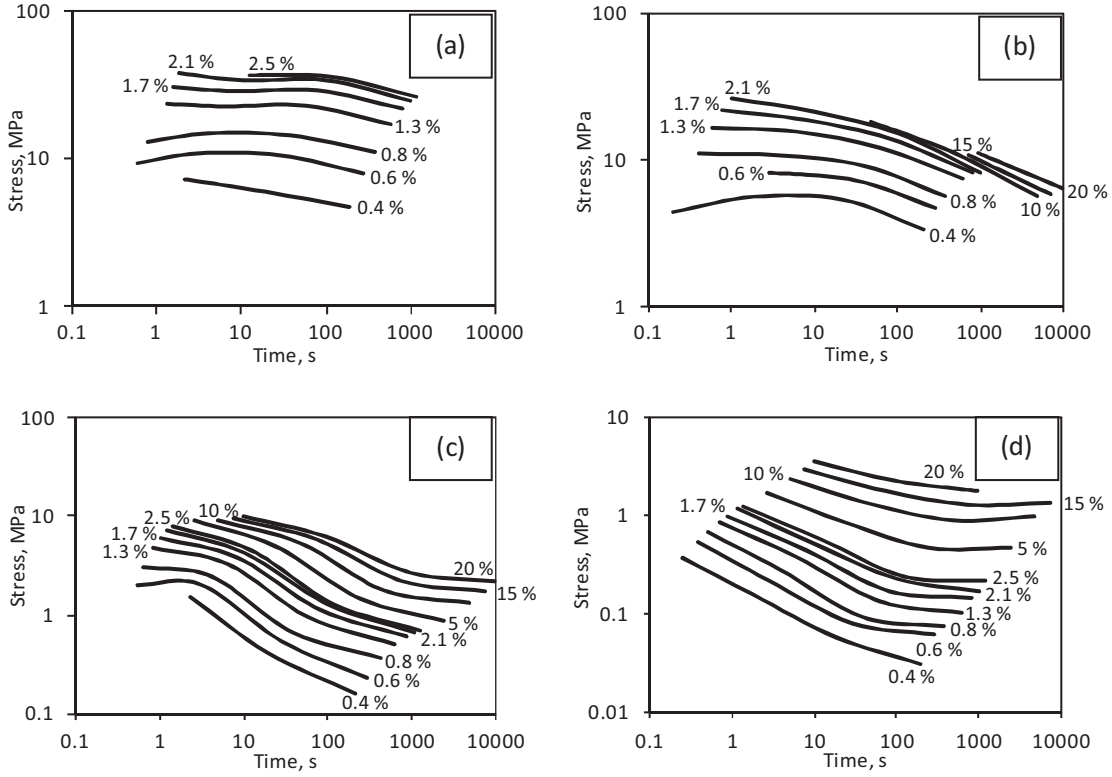

Fig. 9. Iso-strain plots of stress versus time for paint PE1H20 where the axes are in logarithmic scale. Data obtained at 15 °C (a), 25 °C (b), 35 °C (c) and 45 °C (d).

relaxation tests (distribution of relaxation times, determined in Section 5.4) and multi-frequency DMA (TTS constants, determined in Section 5.2). The hyper-elastic constants found in the Ogden equation (Eq. (10)) are used as optimisation parameters, with their values determined so that the constraint in Eq. (9) is satisfied. For the optimisation, the root mean square error (RMSE) in the model prediction was minimised by use of the Solver routine in Excel. The three-term form of the Ogden equation is used here, and therefore six hyper-elastic parameters are determined. Additionally, Eq. (7) requires knowledge of the polymer's glassy and rubbery modulus ($E(0)$ and E_e respectively), which have been measured directly from DMA. Summing up, a total of fourteen parameters are used in the modelling of the tensile behaviour of the paints, eight of which have been determined from stress relaxation and DMA, and another six are obtained from fitting the model to the tensile data.

Experimental tensile curves obtained at temperatures between approximately T_g and $T_g + 20\,^{\circ}C$ are plotted in Fig. 10 along with predictions from Eq. (7). At each temperature the distribution of relaxation times is shifted by the previously determined TTS constants. The calibration of the hyper-elastic parameters was performed against the curves obtained at temperatures higher than T_g (e.g. in the case of PE1H20 these are the curves at 40 and 45 °C); i.e. in every case the sum of the RMSEs at $T > T_g$ was minimised. The decision to exclude the lowest temperature from the optimisation is discussed below. The values of the Ogden parameters are shown in Table 3. It can be seen that the obtained constants generally violate the requirement for $\mu_j a_j > 0$. The basis of this requirement is that by constraining the constants to positive values, a positive value for the strain energy density function of the material is ensured. However, Ogden notes [36] that for $j \geq 3$, the requirement for positive strain energy density can be satisfied even if some of $\mu_j a_j$ are negative. Here, solutions of the Ogden strain energy density function were obtained in uniaxial extension (and compression), equibiaxial extension and simple shear, using the constants given in Table 3 and in every case the strain energy density was found to remain positive for stretch ratios that ranged from 0.1 to 10. Therefore the obtained values are considered to satisfy the stability requirement, even if the products $\mu_j a_j$ are negative.

For each paint in Fig. 10, along with the full stress–strain curves, a zoom-in at low strains is shown. A very good agreement is seen between model and experiment at small strains, where changes in chain-conformation are not significant enough to influence the mechanical response. The insensitivity of the prediction to the hyper-elastic part of the model at these low strains, is demonstrated by substituting the hyper-elastic part with a linear-elastic, Hookean part. This is shown for paint PE1H20 in Fig. 11(a), where the Ogden and Hookean solutions are compared. Clearly up to 5% strain the two solutions yield very similar results. Therefore the small strain data suggest that the visco-elastic component of the model works well, and therefore the initial mechanical response can be predicted with confidence by using a total of eight independently obtained parameters, as shown in Table 2.

At larger strains the quality of the fit depends strongly on the hyper-elastic component of the model. This is demonstrated in Fig. 11(b), where the linear-elastic solution is seen to fail completely in capturing the shape of the stress versus strain curves at large strains. When the model predictions are compared to the full experimental tensile curves of the paints, the quality of the fit is seen to vary with formulation and temperature. With the exception of PE1H30, the model appears to capture the experimental

Table 3
Ogden parameters of formulations PE1H10-30, PE2H20 calibrated with the use of tensile data at approximately $T_g + 5\,^{\circ}C$ and $T_g + 10\,^{\circ}C$.

Formulation	μ_1	α_1	μ_2	α_2	μ_3	α_3
PE1H10	3111	0.82	325	−4.32	−32	−13.99
PE1H20	3100	−0.91	218	0.77	−613	−6.57
PE1H30	3107	−1.64	218	−1.51	−613	−11.25
PE2H20	3095	0.74	780	−1.3	−0.03	−20.2

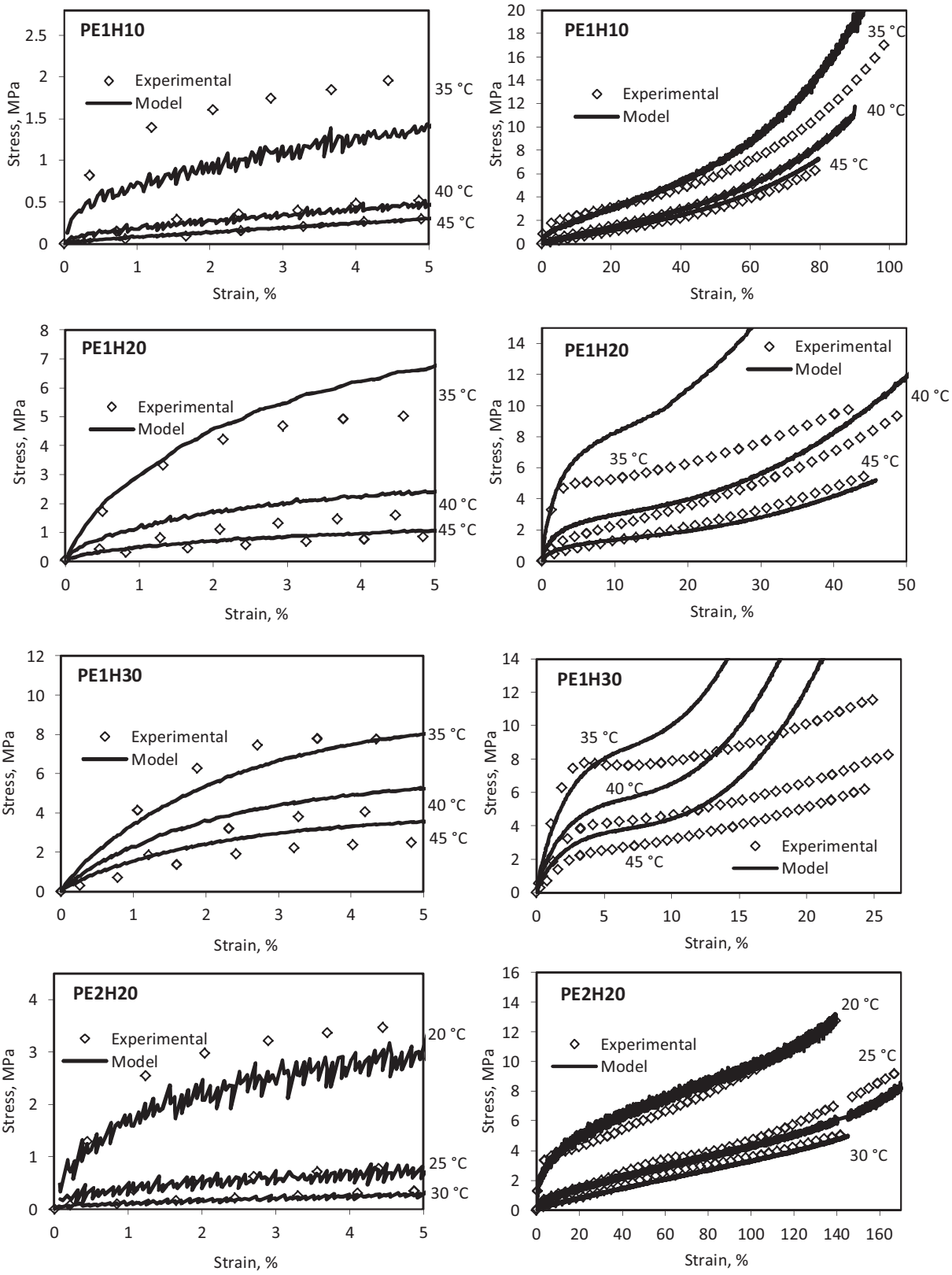

Fig. 10. Stress–strain plots obtained experimentally and from Eq. (7) at different temperatures. Plots on the left show the agreement between model and experiment at small strains, while plots on the right cover the entire strain range.

data better with increasing testing temperature. This might have been expected as the large-strain part of the model was built to capture the hyper-elastic behaviour of rubbers. Therefore it is at the highest testing temperatures that the materials approach the rubbery regime where the model performs best. At lower temperatures the samples showed varying degrees of ductility with clear yield points and in one case (PE1H30) cold-drawing. Under such conditions the distribution of relaxation times is known to depend

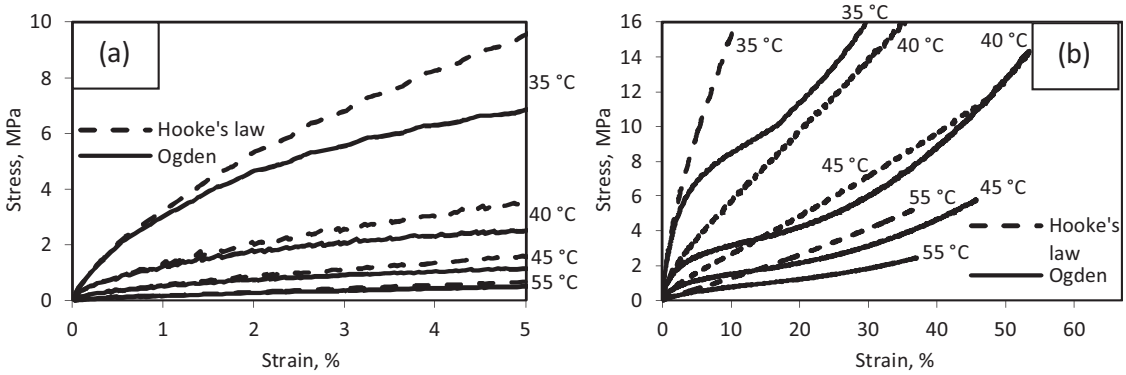

Fig. 11. Comparison, at small (a) and large strains (b), between the predictions from Eq. (7) when σ_0 follows the Ogden model and when it follows Hooke's law for linear-elastic solids.

on the level of stress and on the non-equilibrium structure of the polymer glass [37]. Therefore the inability of the model to cope with yield behaviour was expected, and this is why it was chosen to calibrate the hyper-elastic constants at temperatures above T_g where the material behaviour approached the rubbery regime. In the case of PE1H30, the high cross-link density of the paint resulted in a broad glass transition (reflected also in the width of the relaxation), meaning that even at temperatures above T_g the paint behaved in a ductile manner. This is why the comparison between the model and the experimental data is poor at all temperatures. A model capable of capturing the behaviour of ductile polymers has been proposed by Buckley and co-workers (see for example [37–39]). Future work will focus on the application of such models to the materials at hand, in order to obtain a suitable description of the paint mechanical response throughout the entire temperature range.

6. Conclusions

The visco-elastic behaviour of polyester-based HMMM-cross-linked coatings has been investigated. In particular, simple mechanical tests were performed in order to obtain the constants required for the modelling of the time and strain-dependent mechanical response of the paints under uniaxial tension. The equivalence between the effects of time and temperature was quantitatively determined at small strains, with the use of multi-frequency DMA and the standard Arrhenius and WLF time–temperature superposition treatments. More importantly it was found possible to extend the application of these DMA-determined TTS constants to the ultimate properties of the paints; i.e. to their failure stress and failure strain. This facilitates the determination of the failure properties of the materials at loading rates which would otherwise be very difficult to achieve and is an important result for the coil-coatings industry where paints are expected to be exposed to high loading rates during the forming process.

The distributions of relaxation times of the paints were determined through relaxation tests. These showed a distinct broadening of the relaxation with cross-link density. This is an important finding as it suggests that it is possible to predict the effect of increases in the cross-link density of the materials on their relaxation behaviour. A more formal, quantitative, statement of this relationship would be highly desirable as it would further reduce the amount of testing necessary for the determination of the mechanical response of coatings. The results presented in this study suggest that any such quantitative approach, will need to account for the following key trends with increasing cross-link density: the broadening of the distribution of relaxation times, the increase in rubbery modulus and the decrease in the failure strain of the paint.

Finally, a hybrid visco-elastic/hyper-elastic model was used to capture the tensile stress–strain behaviour of the paints. For the visco-elastic part of the model the parameters determined through the DMA and relaxation tests were used directly, while the constants associated with the hyper-elastic component of stress were calibrated against the experimental data. The agreement between model prediction and experiment was particularly good at low strains (up to approximately 5% strains), signifying the success of the visco-elastic component in capturing the behaviour of the paints. At larger strains the agreement was good in those cases where the stress–strain curves resembled more closely the mechanical behaviour of rubbers, i.e. when no clear yield point and significant strain hardening were observed. When the mechanical response was that of ductile plastics, with yield followed by cold drawing, the agreement between model and experimental data became poor. This was expected as entropic effects due to changes in chain conformation are only partly responsible for the mechanical response of ductile polymers at large strains. A more complete model would also take into account changes in the relaxation behaviour with the level of stress, as well as effects from the non-equilibrium structure of the polymer glass. Such models will be the focus of a future investigation.

References

[1] S. Paul, Types of coatings, in: S. Paul (Ed.), Surface Coatings: Science and Technology, John Wiley and Sons, Chichester, UK, 1996, pp. 659–660.
[2] M. Schmitthenner, Eur. Coat. J. (9) (1998) 618–625.
[3] K. Ueda, T. Amari, H. Kanai, et al., Prog. Org. Coat. 43 (4) (2001) 233–242.
[4] K. Ueda, H. Kanai, T. Amari, Prog. Org. Coat. 45 (2–3) (2002) 267–272.
[5] K. Ueda, H. Kanai, T. Amari, Prog. Org. Coat. 45 (1) (2002) 15–21.
[6] E.W.S. Hagan, M.N. Charalambides, C.R.T. Young, et al., Prog. Org. Coat. 69 (1) (2010) 73–81.
[7] E.W.S. Hagan, M.N. Charalambides, C.R.T. Young, et al., Polymer 52 (7) (2011) 1662–1673.
[8] E.W.S. Hagan, M.N. Charalambides, C.T. Young, et al., Mech. Time-Depend. Mater. 13 (2) (2009) 149–161.
[9] J.D. Ferry, Viscoelastic Properties of Polymers, 2nd ed., John Wiley and Sons, New York, 1970.
[10] S.M. Goh, M.N. Charalambides, J.G. Williams, Mech. Time-Depend. Mater. 8 (3) (2004) 255–268.
[11] N.W. Tschoegl, Mech. Time-Depend. Mater. 1 (1) (1997) 3–31.
[12] N.K. Dutta, G.H. Edward, J. Appl. Polym. Sci. 66 (6) (1997) 1101–1115.
[13] K.S. Cole, R.H. Cole, J. Chem. Phys. 10 (1942) 98–105.
[14] K.S. Cole, R.H. Cole, J. Chem. Phys. 9 (4) (1941) 341–351.
[15] C. Friedrich, H. Braun, Rheol. Acta 31 (4) (1992) 309–322.
[16] D.J. Plazek, J. Rheol. 40 (1996) 987–1014.
[17] M.L. Williams, R.F. Landel, J.D. Ferry, J. Am. Chem. Soc. 77 (14) (1955) 3701–3707.
[18] J.J. Aklonis, W.J. MacKnight, Introduction to Polymer Viscoelasticity, 2nd ed., John Wiley and Sons, New York, 1983.
[19] T.L. Smith, Trans. Soc. Rheol. 6 (1) (1962) 61–80.
[20] M.C. Boyce, E.M. Arruda, Rubber Chem. Technol. 73 (3) (2000) 504–521.
[21] L.R.G. Treloar, The Physics of Rubber Elasticity, Oxford University Press, London, UK, 1949.

[22] L.R.G. Treloar, H.G. Hopkins, R.S. Rivlin, et al., Proc. Roy. Soc. Lond. Ser. A: Math. Phys. Sci. 351 (1666) (1976) 301–330.
[23] R.W. Ogden, Proc. Roy. Soc. Lond. Ser. A: Math. Phys. Sci. 326 (1567) (1972) 565–584.
[24] P.A. Przybylo, E.M. Arruda, Rubber Chem. Technol. 71 (4) (1998) 730–749.
[25] E. Twizell, J. Austral. Math. Soc. Ser. B 24 (424–434) (1983) C646.
[26] E.W.S. Hagan, The Viscoelastic Properties of Latex Artist Paints, Imperial College London, UK, 2009, PhD in Mechanical Engineering.
[27] E.M. Arruda, M.C. Boyce, R. Jayachandran, Mech. Mater. 19 (2–3) (1995) 193–212.
[28] T.L. Smith, J. Polym. Sci. A: General Papers 1 (12) (1963) 3597–3615.
[29] F. Bueche, J.C. Halpin, J. Appl. Phys. 35 (1) (1964) 36–41.
[30] R.F. Landel, R.F. Fedors, Rubber Chem. Technol. 40 (1967) 1049–1059.
[31] R.E. Whittaker, Polymer 13 (4) (1972) 169–173.
[32] J.A.C. Harwood, A.R. Payne, J. Appl. Polym. Sci. 12 (4) (1968) 889–901.
[33] A.R. Payne, R.E. Whittaker, J. Appl. Polym. Sci. 15 (8) (1971) 1941–1948.
[34] J.K.W. Glatz-Reichenbach, L.J. Sorriero, J. Fitzgerald, Macromolecules 27 (6) (1994) 1338–1343.
[35] C.M. Roland, Macromolecules 27 (15) (1994) 4242–4247.
[36] R.W. Ogden, G. Saccomandi, I. Sgura, Comput. Mech. 34 (6) (2004) 484–502.
[37] C.P. Buckley, D.C. Jones, Polymer 36 (17) (1995) 3301–3312.
[38] D.S.A. De Focatiis, J. Embery, C.P. Buckley, J. Polym. Sci. B: Polym. Phys. 48 (13) (2010) 1449–1463.
[39] J.J. Wu, C.P. Buckley, J. Polym. Sci. B: Polym. Phys. 42 (11) (2004) 2027–2040.